IEEE Access
Multidisciplinary ⋮ Rapid Review ⋮ Open Access Journal

Received March 14, 2022, accepted March 29, 2022, date of publication April 8, 2022, date of current version April 15, 2022.

Digital Object Identifier 10.1109/ACCESS.2022.3165854

Printed Dipole Antenna Array With Reconfigurable Feeding Network for Wide Elevation Angle of U2X Communications

YE-YEONG JEONG[1], SEONG-HYEOP AHN[2], (Student Member, IEEE), JINHWAN KOH[2], (Member, IEEE), AND WANG-SANG LEE[2], (Senior Member, IEEE)

[1]Ace Technologies Corporation, Incheon 22013, Republic of Korea
[2]Department of Electronic Engineering, Gyeongsang National University, Jinju 52828, Republic of Korea

Corresponding author: Wang-Sang Lee (wsang@gnu.ac.kr)

This work was supported by the National Research Foundation of Korea (NRF) grant funded by the Korea Government [Ministry of Science and ICT (MSIT)] under Grant 2019R1C1C1008102.

ABSTRACT In this paper, a printed dipole antenna array with reconfigurable feeding network for wide elevation angle of U2X communications is presented. The proposed array consists of a printed 8-element dipole antenna array in the top substrate, two supports with a tapered balun and two reflectors with the reconfigurable feeding network in the bottom substrate. To achieve high gain and wide beam coverage, the proposed reconfigurable feeding network consists of single-pole double-throw (SPDT) switches, single-pole three-throw (SP3T) switches, Wilkinson power dividers, and hybrid couplers. The proposed array antenna forms a 3 × 3 beam consisting of broadside and end-fire beams based on the x- and y-axis using a reconfigurable feeding network. The measured impedance bandwidth, peak gain, and half-power beamwidths (HPBWs) at ϕ=0° and ϕ=90° of the proposed array are approximately 1250 MHz (25%), 7.9 dBi, 197° and 100°, respectively. The overall volume size of the proposed array is 75 × 96×21 mm^3 ($1.3\lambda_0 \times 1.6\lambda_0 \times 0.4\lambda_0$ at 5.1 GHz).

INDEX TERMS Low-profile, printed dipole antenna array, reconfigurable feeding network, wide beam coverage, U2X communications.

I. INTRODUCTION

Recently, in the era of the 4th industrial revolution, 'unmanned vehicles' are rapidly emerged. Unmanned vehicles are defined as mobile vehicles that can recognize the external environment, judge the situation by itself, move, and perform work when necessary [1]. According to the operating environment, unmanned vehicles are classified into unmanned aerial vehicles (UAVs), unmanned ground vehicles, and unmanned marine vehicles. Among them, the UAVs are often called as drones and can be controlled without human onboard [2]. UAVs have advantages such as ease of deployment, low maintenance cost, high mobility, and ability to hover [3]. Historically, the global UAV market has grown around the military applications deployed in hostile territory for remote surveillance and armed attack, to reduce the pilot losses [4]- [5]. In recent years, due to the advancement of UAV's manufacturing technologies and reducing cost, expansion into civilian markets such as agriculture, mining, security, real-time monitoring, remote sensing, delivery of goods, and energy industry, aerial inspection, photography, traffic control, and telecommunications is actively taking place [6]– [7]. In order for UAV to be used in various applications, the customized antenna for reliable and stable UAV-based wireless communications is required [8].

There are several conditions to consider when developing an antenna for UAV communications. First, a low-profile structure and low weight are required for camouflage, efficient power management and small air resistance [6]– [9]. And in order to balance the UAVs up, down, left and right, the antenna also needs a symmetrical balance structure [10]. Finally, in order to avoid discontinuous communication between UAVs and various devices, and to improve communication efficiency, UAVs need not only high-gain beams, but also wide steering ranges to counteract the three-dimensional

The associate editor coordinating the review of this manuscript and approving it for publication was Tawfik Al-Hadhrami.

motion of aerial vehicles and handsets [11]– [12]. Research has been conducted on an antenna for UAV communications that satisfies these conditions [13]– [17]. In [13], an omni-directional antenna with a low height using a buried unipolar patch antenna was implemented by making like the radiation characteristics of a monopole. [14] is a helical antenna, and the antenna size is effectively reduced by using hexaferrite-glass composite as the antenna core. In [15], a low-profile antenna was implemented using a magnetic dipole antenna. [16] is a conical patch antenna array using the flexible substrate and has wide elevation angles and high gain. [17] is a CP patch antenna with small size and uniform elevation angle. The antennas of [14]– [17] all have low height and operate at 2.45 GHz. The reason why these antennas are designed to operate at 2.45 GHz is that the conventional UAVs have been communicated in the S-band with 2.45 GHz as the center frequency. However, since this frequency band is the same frequency band as Wi-Fi, there is a possibility of crosstalk. If the signal of the UAV and Wi-Fi signal are confused, the UAV may become out of control or malfunction, leading to an accident or damage. Therefore, it is necessary to allocate a dedicated frequency band for UAVs. In 2012, through the World Radio Communication Conference (WRC-12) under the International Telecommunication Union (ITU), the frequency band for wireless communication of UAVs (5.03 to 5.091 GHz) and the frequency band for missions (5.091 to 5.15 GHz) has been assigned. Accordingly, studies have been conducted on high-gain antennas with low air resistance operating in the 5 GHz band [18]– [20].

In [18], an antenna with very high gain is implemented using a patch antenna array, phase shifters and amplifiers. [19] produced an antenna with a high gain and wide elevation angle using Yagi-Uda dipole antenna array. [20] achieved a high gain and wide elevation angles by implementing a relatively low-profile antenna by using a meander monopole and a circular patch antenna. Previous studies on antennas for UAV communications operating in the 5 GHz band were also conducted. One of our previous works was a wide beam coverage dipole antenna array with parasitic elements [21]. The proposed array has a wide elevation angle due to the influence of the parasitic element, but there is a limitation to cover the whole hemispherical region due to single beam. Another previous work was a UAV communication antenna array with a 3 × 2 switched beamforming network that forms three beams [22].

The proposed array formed three beams to improve the elevation angle and the gain. The main beam directions(ϕ) of the three beams are -90°, 0°, and 90° respectively. The proposed array has a wide elevation angle with respect to the x-axis and can transmit and receive signals of vertical and horizontal polarization. In [23], the limitations of the previous two studies were supplemented by forming a quadruple-mode beam. The proposed array forms not only vertical polarization and horizontal polarization, but also polarization inclined at 45° and polarization inclined at 135°, so it has the advantage of being able to transmit and receive at various angles. In addition, it has the advantage of having a uniform beam elevation angle in the elevation plane by forming a quadruple mode beam. However, for stable communication, an array antenna with higher gain, wider beam elevation, and various polarization directions than the antennas of [18]– [23] is required. Therefore, in this paper, to improve the performance of previously proposed antennas, we propose an 8-array dipole antenna with a wide elevation angle and high gain various polarization directions using a linear array antenna theory, parasitic element, and reconfigurable feeding network. Simulations have been conducted using CST Microwave Studio [24] which show good agreement with experiments. Fig. 1 describes the proposed array with wide-coverage beam patterns in the U2X communications.

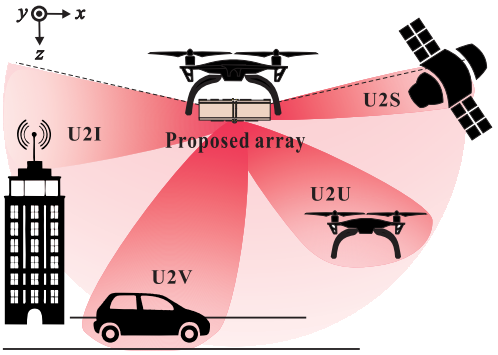

FIGURE 1. Radiation patterns of the proposed array with the U2X communications.

II. ANTENNA ARRAY DESIGN THEORY

A typical half-wave dipole antenna has an omni-directional radiation pattern and a low gain of 2.15 dBi. In order to use a half-wave dipole antenna for UAV communications, it must be designed to improve gain and have a wide radiation pattern for θ. To satisfy the design conditions, by applying the linear array antenna theory to the dipole array antenna, a radiation pattern having a high gain and wide elevation angles can be formed.

A. N-ELEMENT LINEAR ANTENNA ARRAY THEORY

In order to obtain the radiation pattern of the N-elements linear antenna array, as shown in Fig. 2, N-elements with current applied horizontally on the y-axis are arranged with a distance of d on the z-axis [25]. The array factor for this can be expressed by (1).

$$AF = \sum_{n=1}^{N} e^{j(n-1)\Psi} \tag{1}$$

where

$$\Psi = kdcos\theta + \beta \tag{2}$$

In (2), k, θ, and β are defined as the wave number, angle between the observation point and the antenna array axis, and

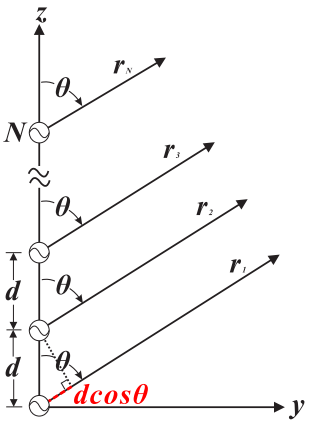

FIGURE 2. N-element antennas arranged at intervals of *d* on the *z*-axis.

phase of each antenna, respectively. (3) can be obtained by subtracting the expression (1) multiplied by $e^{j\Psi}$ from (1).

$$(1 - e^{j\Psi})AF = (1 - e^{jN\Psi}) \tag{3}$$

AF in (1) is (1-$e^{jN\Psi}$)/(1-$e^{j\Psi}$) through (3). If (3) is arranged and normalized using a sinusoidal function, the array factor of (4) for an N-elements linear antenna array can be obtained.

$$(AF)_n = \frac{1}{N}\left[\frac{sin\left(\frac{N}{2}\Psi\right)}{sin\left(\frac{1}{2}\Psi\right)}\right] \tag{4}$$

The maximum radiation of an array directed normal to the axis of the array [broadside; $\theta = 90°$ of Fig. 2] can be formed through the arrayed antennas and the array factor of (4). To optimize the design, the maxima of the single element and of the array factor should both be directed toward θ=90°. Referring to (4), the first maximum of the array factor occurs when

$$\Psi = kdcos\theta + \beta \ = 0 \tag{5}$$

Since $\theta = 90°$, then $\beta = 0$. Thus to have the maximum of the array factor of a uniform linear array directed broadside to the axis of the array, it is necessary that all the elements have the same phase excitation (in addition to the same amplitude excitation). To avoid any grating lobe and occur only maximum at broadside, the spacing between the elements should be λ/4.

Instead of having the maximum radiation broadside to the axis of the array, it may be desirable to direct it along the axis of the array (end-fire). As a matter of fact, it may be necessary that it radiates toward only one direction (either $\theta = 0°$ or $\theta = 180°$ of Fig. 2). Substituting $\theta = 0°$ (or 180°) for (2), then Ψ = -kd (or kd). Thus end-fire radiation is accomplished when β = -kd (for $\theta = 0°$) or kd ($\theta = 180°$). If the element separation is $d = \lambda/2$, end-fire radiation exists simultaneously in both directions ($\theta = 0°$ and $\theta = 180°$). To have only one end-fire maximum and to avoid any grating lobe, the spacing between the elements should be λ/4.

$$(AF)_n = \frac{1}{N}\left[\frac{sin\left[\frac{Nkd}{2}(cos\theta \mp 1)\right]}{sin\left[\frac{kd}{2}(cos\theta \mp 1)\right]}\right] \tag{6}$$

When all the elements have the same amplitude excitation and the phase difference between unit antennas is 90° and -90°, respectively, the array factor of the end-fire beam is defined by the equation (6). According to (6), the main beam direction is $\theta = 0°$ (or $\theta = 180°$) when the phase difference between the unit antennas is 90° (or -90°). The radiation patterns of the maximum broadside and end-fire beams are shown in Fig. 3.

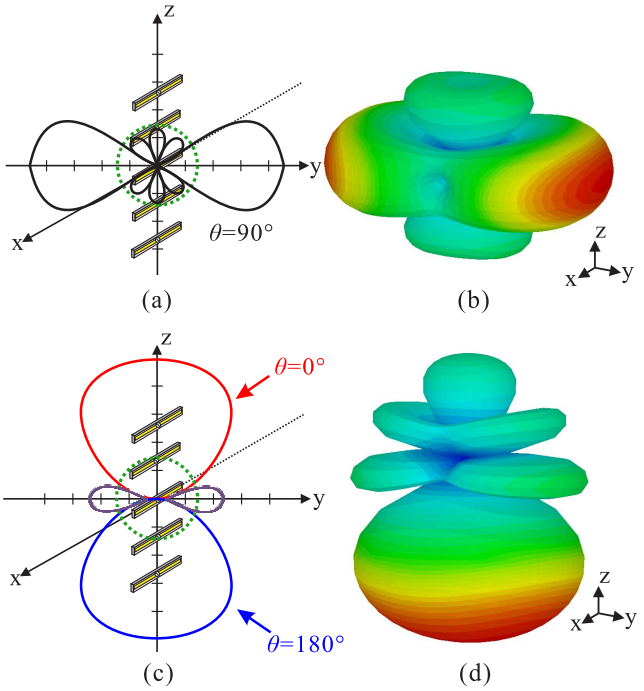

FIGURE 3. Radiation patterns: (a)-(b) 2D or 3D radiation patterns of a broadside beam (c) 2D radiation patterns of end-fire beams (d) 3D radiation pattern of a end-fire beam when $\theta = 180°$.

B. OPERATIONAL PRINCIPLE OF THE PROPOSED ARRAY

The dipole array antenna can form a broadside beam and two end-fire beams using the linear array antenna theory [22]. Theoretically, when there is no phase difference of each unit antenna, the radiation pattern of the array antenna radiates perpendicular to the array axis, but the rear radiation is reduced due to effect of the metal reflector placed behind the antenna, so Fig. 4(a). As in, it radiates only along the *z*-axis. When the phase difference between unit antennas is -90° or +90°, the end-fire beam radiates to the +*x* and -*x* axes, respectively, but contrary to the theory, the radiation to the -*z* axis is reduced by installing a metal reflector behind the antenna. As shown in Figs. 4(b)–(c), the main beam angle of each radiation pattern is inclined by about 45° along the *z*-axis. In the previous study, one broadside beam and two end-fire beams were formed with a 1 × 4 array antenna in the *x*-axis direction by applying the antenna theory. However,

TABLE 1. Each distribution of amplitudes and phase variations with regard to the input modes.

Distributions		Mode 1	Mode 2	Mode 3	Mode 4	Mode 5	Mode 6	Mode 7	Mode 8	Mode 9
SPDT-1 to SPDT-4 States		P2 / P5			P2 / P4			P3 / P4		
SP3T-1 or SP3T-2 States		P6 / P9	P7 / P10	P8 / P11	P6 / P9	P7 / P10	P8 / P11	P6 / P9	P7 / P10	P8 / P11
Output (Ampl., Phase)	A1	1/2, 0°	$1/2\sqrt{2}$, 90°	-	1/2, 0°	$1/2\sqrt{2}$, 90°	-	1/2, 90°	$1/2\sqrt{2}$, 180°	-
	A2	1/2, 90°	$1/2\sqrt{2}$, 0°	-	1/2, 90°	$1/2\sqrt{2}$, 0°	-	1/2, 180°	$1/2\sqrt{2}$, 90°	-
	A3	-	$1/2\sqrt{2}$, 0°	1/2, 90°	-	$1/2\sqrt{2}$, 0°	1/2, 90°	-	$1/2\sqrt{2}$, 90°	1/2, 180°
	A4	-	$1/2\sqrt{2}$, 90°	1/2, 0°	-	$1/2\sqrt{2}$, 90°	1/2, 0°	-	$1/2\sqrt{2}$, 180°	1/2, 90°
	A5	1/2, 90°	$1/2\sqrt{2}$, 180°	-	1/2, 0°	$1/2\sqrt{2}$, 90°	-	1/2, 0°	$1/2\sqrt{2}$, 90°	-
	A6	1/2, 180°	$1/2\sqrt{2}$, 90°	-	1/2, 90°	$1/2\sqrt{2}$, 0°	-	1/2, 90°	$1/2\sqrt{2}$, 0°	-
	A7	-	$1/2\sqrt{2}$, 90°	1/2, 180°	-	$1/2\sqrt{2}$, 0°	1/2, 90°	-	$1/2\sqrt{2}$, 0°	1/2, 90°
	A8	-	$1/2\sqrt{2}$, 180°	1/2, 90°	-	$1/2\sqrt{2}$, 90°	1/2, 0°	-	$1/2\sqrt{2}$, 90°	1/2, 0°
Beam Direction (θ)		End-fire (-y-axis, θ=60°)			Broadside (center, θ=0°)			End-fire (y-axis, θ=60°)		

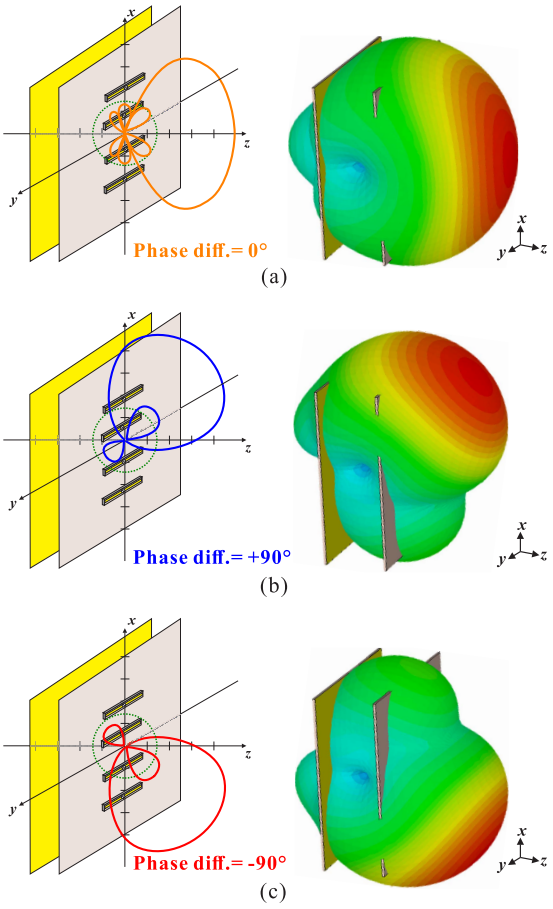

FIGURE 4. 3D radiation patterns with the metal reflector: (a) radiation pattern of broadside beam when theta = 0°, (b)-(c) radiation pattern of end-fire beam when theta = +90° or −90°.

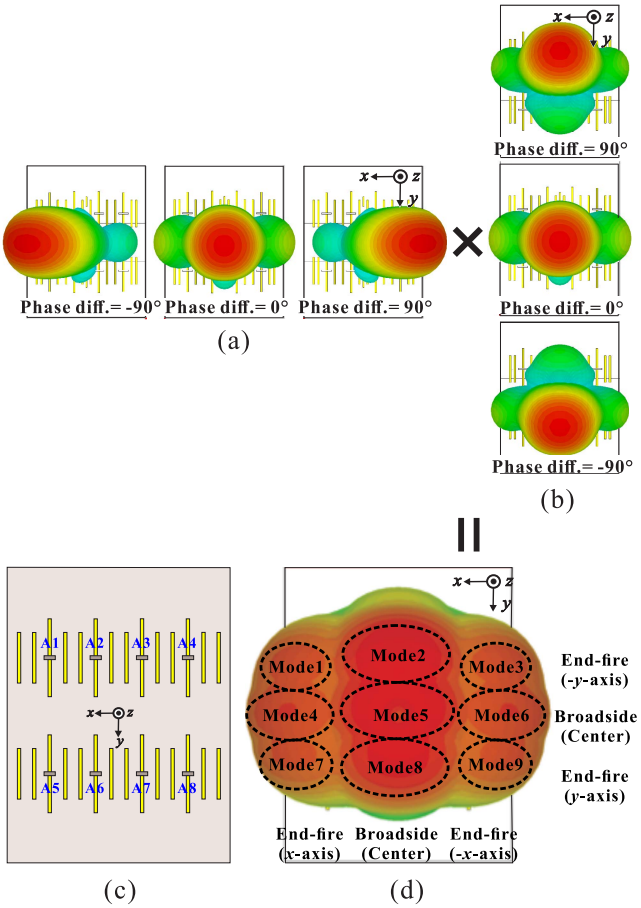

FIGURE 5. Multi-beam forming principle of the proposed array antenna: (a)-(b) broadside beams and end-fire beams radiating about the *x*-axis or *y*-axis, (c) a top view of the proposed array antenna (d) 3D radiation patterns at 5.1 GHz on the *xy* plane in total modes.

in this case, there is a limitation that the beam width of the *yz*-plane is relatively narrow. To overcome the limit of the previous antenna, in this paper, the 2 × 4 dipole array antenna was designed by placing the 1 × 4 dipole array antenna once more at a distance of about λ/2 in the *y*-axis direction. The 2×4 dipole array antenna can form a broadside beam and an end-fire beam in the *yz*-plane by controlling the phase difference between four antennas in the first row and four antennas in the second row. (Fig. 5). When forming

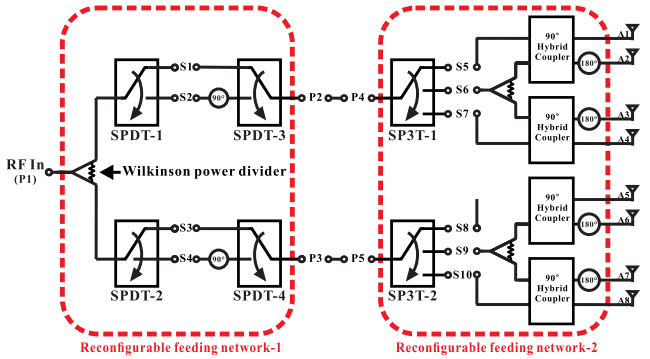

FIGURE 6. Block diagram of the proposed 1 × 8 reconfigurable feeding network.

the beams of modes 1, 4, and 7 in Fig. 5(d), four antennas located in the *x*-axis direction are used (A1, A2, A5, A6). In this case, the reason why eight antennas are not used is that the beam width becomes sharper as the number of array elements increased, and the elevation angles in the *x*-axis direction becomes narrow. Therefore, the elevation angles were widened using only four antennas (A3, A4, A7, A8) located in the *x*-axis direction. By the same principle, beams of mode3, 6, and 9 were formed with 4 antennas located in the -*x*-axis direction. And when implementing mode 2, 5 and 8 radiating from the center of the *x*-axis, all 8 antennas were used to increase the gain. In addition, using the experiment in [21], parasitic elements shorter than the length of the antenna were placed between each antenna. The parasitic element can adjust the directivity of the beam like the waveguide of the Yagi-Uda antenna. Therefore, in this paper, the parasitic element was used to widen the beam width by dispersing the beam of the array antenna (Fig. 5(c)). Therefore, the proposed array antenna has a wide elevation angle and high gain by forming a 9-mode multiple beam using array antenna theories and parasitic elements.

III. PROPOSED ARRAY CONFIGURATION AND ITS DESIGN

A. 1 × 8 RECONFIGURABLE FEEDING NETWORK DESIGN

Table 1 shows each distribution of amplitudes and phase variations with regard to the input modes. A block diagram of 1 × 8 reconfigurable feeding network used in the proposed array is shown in Fig. 6. The proposed reconfigurable feeding network consists of four single-pole-double-throw (SPDT) switches, two single-pole-three-throw (SP3T) switches, three Wilkinson power dividers, and four hybrid couplers. First, in the reconfigurable feeding network-1, there are a transmission line having the shorter electrical length and a transmission line having the longer electrical length by λ/4 (the transmission line with a phase delayed by 90°). One of two transmission lines type is selected through SPDT-1 and SPDT-3 (SPDT-2 and SPDT-4). Accordingly, the phase difference (0° and ±90°) between the dipole antennas in the first row (A1-A4) and the dipole antennas (A5-A8) in the second row is determined through the reconfigurable

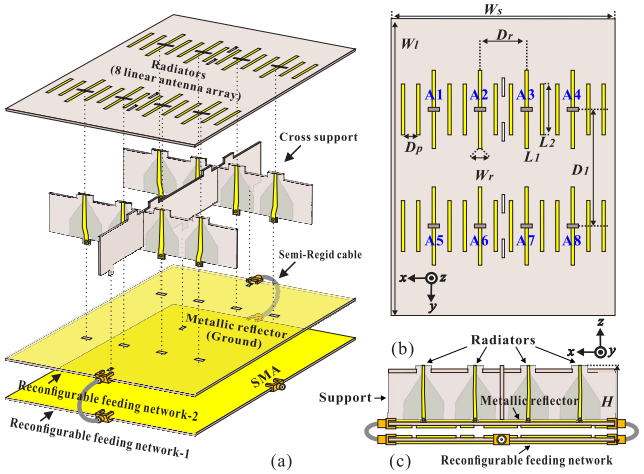

FIGURE 7. Overall configuration of the proposed array: (a) a perspective view, (b) a top view of the radiator with 8 dipole antennas and 20 parasitic elements, and (c) a side view.

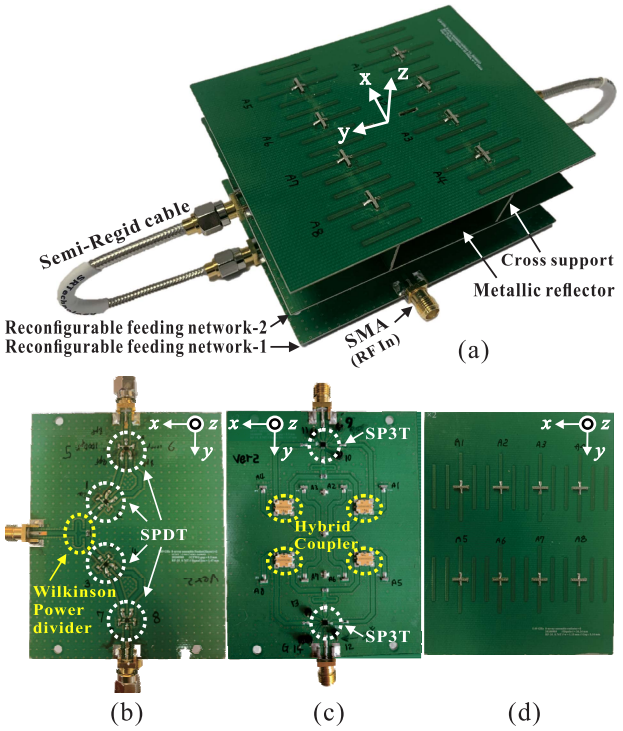

FIGURE 8. Photographs of the array prototype: (a) a perspective view, (b) RF Board of the reconfigurable feeding network-1, (c) RF Board of the reconfigurable feeding network-2, and (d) a top view of the radiators.

feeding network-1. As a result, broadside beams radiating in a direction of 0° and end-fire beams radiating in a direction of ±20° with respect to the *y*-axis ($\phi = 90°$) are formed through the reconfigurable feeding network-1. Reconfigurable feeding network-2 is designed to form a broadside beam radiating in the direction of 0 ° with respect to the *x*-axis like [3] and an end-fire beam radiating in a direction of ±45°. When the P6 mode is selected in SP3T-1, only the outputs A1(0°) and A2(90°) are operated through the coupler and the transmission line with a phase delayed by

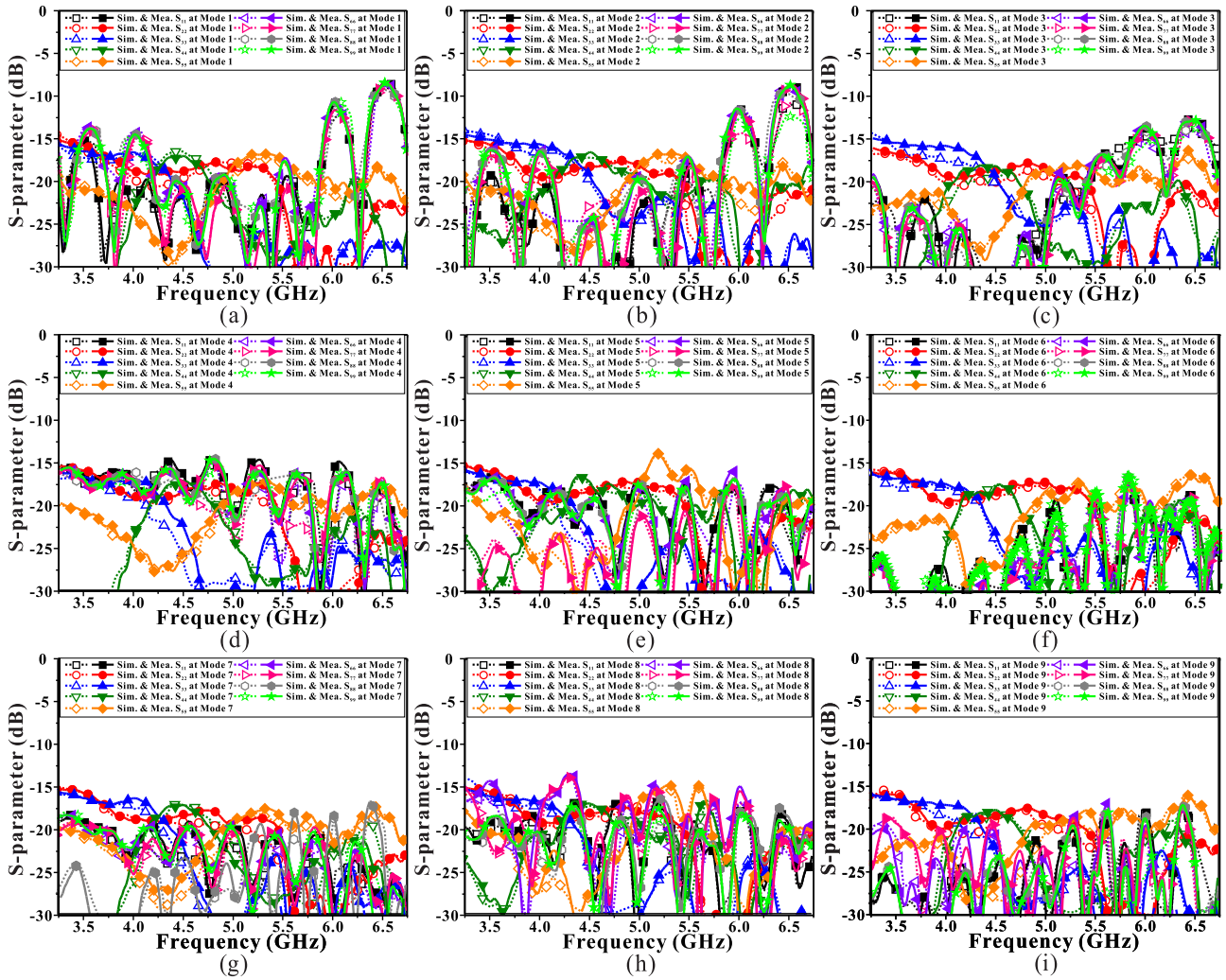

FIGURE 9. Simulated and measured reflection coefficients of the proposed reconfigurable feeding network with regard to different modes: (a)–(i) simulated and measured reflection coefficients.

180° to form an end-fire beam radiating to the x-axis. Next, when the P7 mode is selected in SP3T-1, power is distributed to two hybrid couplers by the Wilkinson power divider, so that the four outputs (A1-A4) have a phase difference of 90°, 0°, 0°, and 90°. This results in a centrally radiating broadside beam. Finally, when the P8 mode is selected in SP3T-1, only the outputs A3(90°) and A4(0°) are operated through the hybrid coupler and the transmission line with a phase delayed by 180° to form an end-fire beam radiating to the x-axis. The phase and amplitude of A4–A8 according to the state of SP3T-2 are determined in the same way as the control method of A1–A4 by the state of SP3T-1.

B. ANTENNA CONFIGURATION INCLUDING 1 × 8 RECONFIGURABLE FEEDING NETWORK

Fig. 7 represents the overall configuration of the proposed array. The proposed array structure consists of an upper substrate, a middle substrate, lower substrate, and supports as shown in Fig. 7(a). As shown in Fig. 7(b), the horizontal spacing between each antenna element is $1/4\lambda_0$ and the vertical spacing between each antenna element is $1/2\lambda_0$ (D_r = 15.5 mm, D_1 = 36 mm), parasitic elements are placed between radiators at $1/12\lambda_0$ (D_p = 5.2 mm) spacing and used as an important parameter to widen the elevation angle. In addition, the metal reflector is the ground plane of the proposed reconfigurable feeding network and takes part in an important role in reducing backside radiation and improving the radiation gain. The design parameters of the proposed array are H = 21 mm, L_1 = 26.3 mm, L_2 = 17 mm, W_l = 96 mm, W_r = 25.5 mm, W_s = 75 mm. The supports are composed of a microstrip line and a tapered balun for connecting the reconfigurable feeding network and the dipole antennas, as shown in Fig. 7(c). The reconfigurable feeding network-1 and the reconfigurable feeding network-2 are connected through Semi-Regid cables and SMA connectors. All substrates used TACONIC RF-35 (ε_r = 3.5 and tan δ = 0.0018). Their thicknesses are 0.76 mm and the copper thicknesses are 18 μm. The total size of the proposed array is 75 × 96×21 mm^3 ($1.3\lambda_0 \times 1.6\lambda_0 \times 0.4\lambda_0$ at 5.1 GHz).

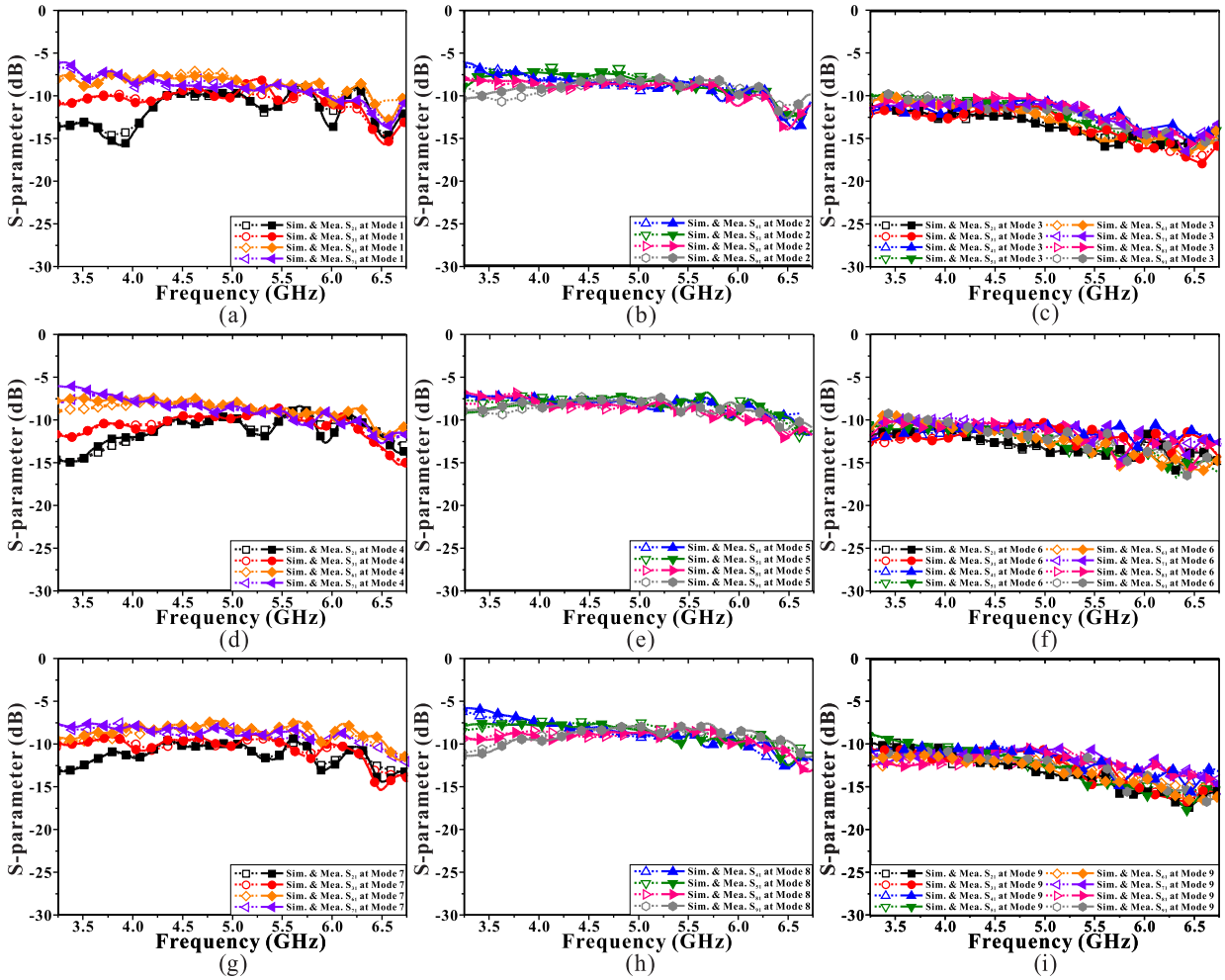

FIGURE 10. Simulated and measured transmission coefficients of the proposed reconfigurable feeding network with regard to different modes: (a)–(i) simulated and measured transmission coefficients.

IV. EXPERIMENTAL VERIFICATIONS

To verify the proposed design, the fully functional prototype of the proposed array in Fig. 8(a) was fabricated. In Figs. 8(b)–(c), the SPDT ([29]) and SP3T ([30]) switches for selecting and making nine linear polarization modes were CG2430 × 3 (absolute maximum input power = 33.5 dBm, 1 dB input compression point = 32 dBm) made by CEL, SKY13408-465LF (absolute maximum input power = 40 dBm, 1 dB input compression point = 34 dBm) made by Skyworks, respectively. The 90° hybrid coupler is CMX55Q03 by RN2 Technologies ([31]). Fig. 8(d) shows the topveiw of the fabricated radiators.

Fig. 9 shows the simulated and measured reflection coefficients of the proposed reconfigurable feeding network with regard to different modes (mode 1 to 9). The S_{11} to S_{99} are the reflection coefficients of the RF input port (P1) and the output ports (A1, A2, A3, A4, A5, A6, A7, and A8), respectively. The measured results have a good agreement with the simulated results. In addition, the reflection coefficients of the proposed reconfigurable feeding network has a measured results of -10dB or less in all modes and within 3.2–6.0 GHz. Therefore, it can be seen that the proposed reconfigurable feeding network operates normally in the 5 GHz band.

Fig. 10 shows the simulated and measured transmission coefficients of the proposed reconfigurable feeding network with regard to different modes (mode 1 to 9). The S_{21} to S_{91} are the transmission coefficients between the RF input port and the output ports, respectively. In modes 1, 4, 7 (Figs. 10(a), (d), (g)) with outputs of A1, A2, A5, and A6, the transmission coefficients is approximately minimum −11.2 dB and maximum −7.3 dB. It is included power loss of two SPDT switches, one SP3T switch, one power divider, and one hybrid coupler, respectively. In modes 2,5,8 (Figs. 10(b), (e), (h)) with outputs of A3, A4, A7, and A8, the transmission coefficients is approximately minimum -9.5 dB and maximum -7.3 dB. It is included power loss of two SPDT switches, one SP3T switch, one power divider, and one hybrid coupler, respectively. In modes 3,6,9 (Figs. 10(c), (f), (i)) with outputs of A1 to A8,

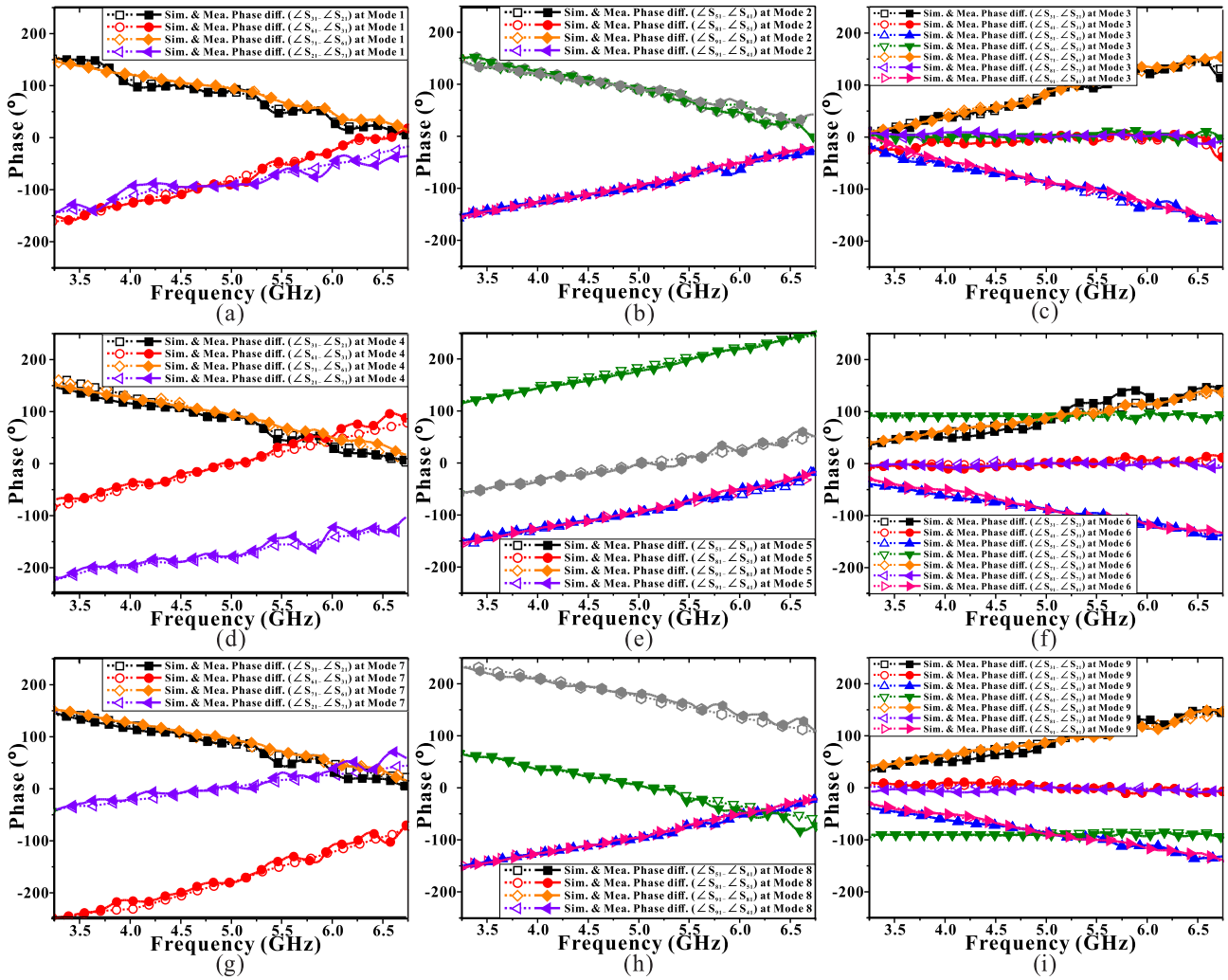

FIGURE 11. Simulated and measured phase differences of the proposed reconfigurable feeding network with regard to different modes: (a)–(i) simulated and measured phase differences.

the transmission coefficients is approximately minimum -13.8 dB and maximum -10.5 dB. It is included power loss of two SPDT switches, one SP3T switch, two power dividers, and one hybrid coupler, respectively. Since the measured results have a good agreement with the simulated results, it can be confirmed that the proposed reconfigurable feeding network operates normally without cross-talk or coupling.

Fig. 11 shows the measured phase differences of the proposed reconfigurable feeding network with regard to different modes (Mode 1 to 9). Referring to Fig. 6, the maximum error of the measured phase difference for each mode is -8.3°, so it can be seen that the intended phase difference was well-formed in the manufactured reconfigurable feeding network. In addition, it can be seen that the proposed reconfigurable feeding network is well designed because the simulated phase difference and the measured phase difference are almost identical.

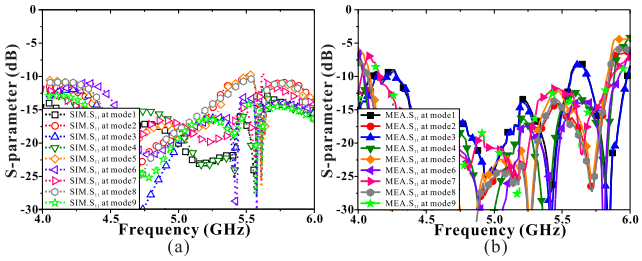

FIGURE 12. Simulated and measured reflection coefficients of the proposed array with regard to different modes: (a) simulated reflection coefficients, (b) measured reflection coefficients.

Figs. 12(a) and (b) are the simulated and measured reflection coefficients for each mode of the fabricated array. The measured results have a good agreement with the simulated results. The measured common 10-dB bandwidth (IBW) of modes 1–9 was measured to be 25% from about 4.4 to 5.7 GHz.

TABLE 2. Comparison between previous works for UAV communications and the proposed array.

Comp.	f_c (GHz)	HPBWs (Elevation Planes)		Bandwidth (%)	Size ($\lambda_0 \times \lambda_0 \times \lambda_0$)	Gain (dBi)	Antenna type
[3]	5.09	180°	75°	17	1.3 × 1 × 0.3	6.7	Dipole antenna array
[13]	0.7	60°	–	6.5	0.23×0.23×0.02	1.9	Monopolar patch antenna
[14]	2.4	60	60	3.7	1.4 × 1.4 × 0.1	4.5	hexaferrite helical antenna array
[15]	2.45	54°	–	4.0	2.0 × 0.4 × 0.06	4.0	microstrip magnetic dipole antenna
[16]	2.4	120°	–	3.4	2 × 1.2 × 0.5	8.3	Conical Conformal Array Antenna
[17]	2.45	90°	90°	0.6	0.4 × 0.4 × 0.01	4.5	Microstrip patch antenna
[18]	5.5	10°	80°	5.5	5.4 × 4.1 × 0.01	24	Phased array
[19]	5.5	150°	150°	28	2.4 × 2.4 × 5	6.3	Yagi-Uda dipole array
[20]	5.09	145°	145°	10.8	1 × 1 × 0.2	5.8	multiple antenna
[21]	5.09	136°	–	15.6	1.6 × 1.1 × 0.3	5.5	Dipole antenna array
[22]	5.09	155°	–	39.3	1 × 0.9 × 0.4	4.3	Dipole antenna array
[23]	5.09	99°	99°	29.6	1 × 1 × 0.3	5.9	Half bow-tie antenna array
Prop.	**5.09**	**197°**	**100°**	**25**	**1.3 × 1.6 × 0.4**	**7.9**	**Dipole antenna array**

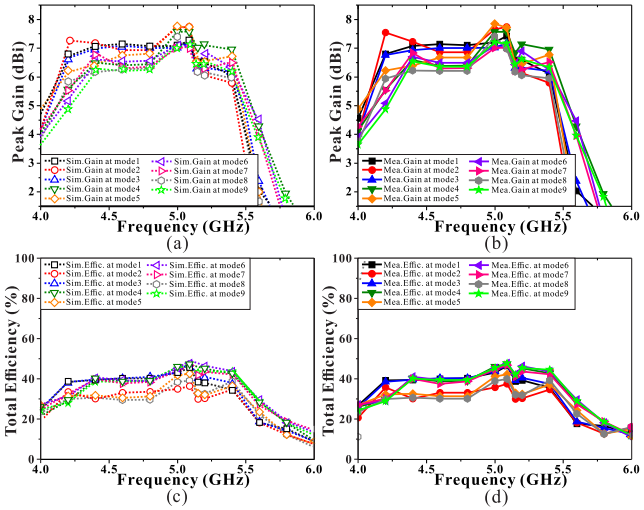

FIGURE 13. Simulated and measured peak gains and total efficiencies of the proposed array with regard to different modes: (a)–(b) simulated and measured peak gains, (c)–(d) simulated and measured total efficiencies.

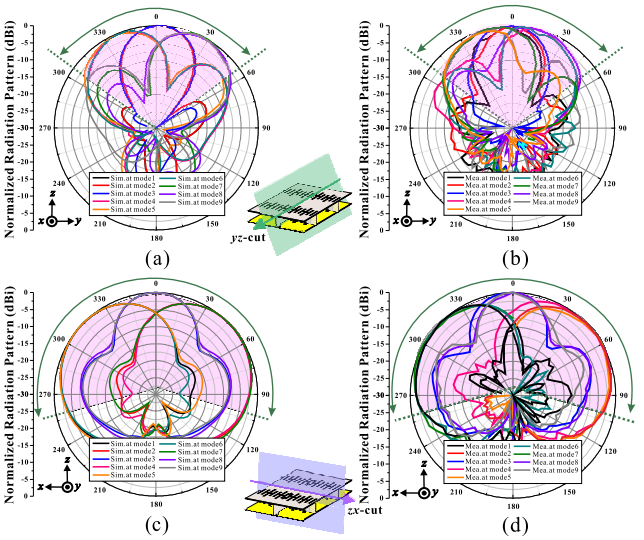

FIGURE 14. Simulated and measured radiation patterns for each mode: (a)–(b) simulated and measured radiation patterns in the *yz*-plane, (c)–(d) simulated and measured radiation patterns in the *zx*-plane.

Figs. 13(a)–(d) show the simulated and measured peak gains and total efficiencies according to the frequency of the fabricated array antenna. When Figs. 13(a) and (b) are compared, it can be seen that the simulated and measured results are almost identical. The minimum gain measured at 5.1 GHz of the fabricated array antenna is 6.8 dBi and the maximum gain is 7.9 dBi. The reason that the minimum gain and the maximum gain differ by about 1.1 dBi is because the maximum gain of the beam emitted by the array is different when 4 antennas are operated and when all 8 antennas are operated. Figs. 13(c) and (d) show the simulated and measured total efficiency for each frequency. The measured results are almost in agreement with the simulated results. The measured total efficiencies at 5.1 GHz from a minimum of 38% to a maximum of 49%. The reason that the total efficiencies do not exceed 50% is that the total efficiencies are lowered due to the loss caused by using the RF switches and the half power loss caused by using the Wilkinson power dividers and hybrid couplers.

Radiation patterns for each mode in the *yz*- and *zx*-plane are shown in Figs. 14(a)–(d). Figs. 14(a)–(b) show the simulated and measured radiation patterns for each mode in the *yz*-plane. When comparing Figs. 14(a) and (b), it can be seen that the simulated radiation patterns and the measured radiation patterns are almost good agreement. Figs. 14(c)–(d) show the simulated and measured radiation patterns for each mode in the *zx*-plane. When comparing Figs. 14(c) and (d), it can be seen that the simulated radiation patterns and the measured radiation patterns are almost identical. The total HPBW of the beam pattern for each mode of the proposed array is 197°.

Table 2 shows a comparison table of the antenna performance of the proposed array antenna and the previous study case. First, the antennas of [13]– [17] cannot all be used in the 5 GHz band, and they have a narrow 10-dB bandwidth, so it seems that there will be limitations in using them for various UAV applications. [18] achieves a high gain by using phase shifters and amplifiers, but has limitations in that it is expensive and has a narrow elevation angle. [19] implements a wide elevation angle using 16 antennas and MCU. However, it has a complex structure and a large size. Previous studies ([21]– [22]) have the disadvantage of having a wide elevation angle only with respect to the x-axis. The antenna [23], which was proposed to improve [21]–[22], has a uniform elevation angle and four multi-beams, thereby eliminating the dead zone. However, it appears that the gain and elevation angle need to be improved. An antenna that can secure the limitations of [13]– [23] is proposed in this paper. The proposed array has a relatively small size, high gain, wide HPBW, and simple structure. In addition, the phase shifter, amplifier, and MCU are not used, which greatly reduces the cost. Therefore, the proposed array has advantages of high gain, wide elevation angle, wide impedance bandwidth, and low cost compared to [13]– [23]. Also, compared with the previously proposed antenna [3], the beam width and gain in the zx-plane and yz-plane were 17°(9.4%), respectively. 40°(66.7%) and 1.2 dBi(17.9%) were improved.

V. CONCLUSION

In this paper, we propose printed dipole antenna array with reconfigurable feeding network for wide elevation angle of U2X communications. The proposed array forms a 3×3 beam using broadside beams and end-fire beams based on the x-axis and y-axis using a reconfigurable feeding network. And the proposed array uses parasitic elements to improve the elevation angle. In addition, in order to improve the gain by reducing backside radiation and to prevent the antenna from being affected by the UAV and the reconfigurable feeding network, the back side of the reconfigurable feeding network was used as a grounded metal plate. Therefore, the proposed array has high gain and wide elevation angle as well as low height and symmetrical structure, so it is expected to have high utility in applications using UAVs.

REFERENCES

[1] Department of Original Technology. (Jan. 2018). *10-Year Roadmap for Unmanned Vehicle Technology Innovation and Growth*. KISTEP. [Online]. Available: https://www.korea.kr/archive/expDocView.do?docId=37916

[2] S. Hayat, E. Yanmaz, and R. Muzaffar, "Survey on unmanned aerial vehicle networks for civil applications: A communications viewpoint," *IEEE Commun. Surveys Tuts.*, vol. 18, no. 4, pp. 2624–2661, 4th Quart., 2016.

[3] Y. Y. Jeong, D. G. Seo, and W. S. Lee, "5 GHz UAV array antenna design with a 3×4 reconfigurable feeding network for wide elevation coverage," *J. Korean Inst. Electromagn. Eng. Sci.*, vol. 31, no. 8, pp. 688–692, Aug. 2020.

[4] Y. Chen and C.-F. Wang, "Electrically small UAV antenna design using characteristic modes," *IEEE Trans. Antennas Propag.*, vol. 62, no. 2, pp. 535–545, Feb. 2014.

[5] Y. Zeng, Q. Wu, and R. Zhang, "Accessing from the sky: A tutorial on UAV communications for 5G and beyond," *Proc. IEEE*, vol. 107, no. 12, pp. 2327–2375, Feb. 2019.

[6] H. Shakhatreh, A. H. Sawalmeh, A. Al-Fuqaha, Z. Dou, E. Almaita, I. Khalil, N. S. Othman, A. Khreishah, and M. Guizani, "Unmanned aerial vehicles (UAVs): A survey on civil applications and key research challenges," *IEEE Access*, vol. 7, pp. 48572–48634, 2019.

[7] J. F. Gonzalez, P. Padilla, J. F. Valenzuela-Valdes, J.-L. Padilla, and M. Sierra-Perez, "An embedded lightweight folded printed quadrifilar helix antenna: UAV telemetry and remote control systems," *IEEE Antennas Propag. Mag.*, vol. 59, no. 3, pp. 69–76, Jun. 2017.

[8] Y. Cui, P. Luo, Q. Gong, and R. Li, "A compact tri-band horizontally polarized omnidirectional antenna for UAV applications," *IEEE Antennas Wireless Propag. Lett.*, vol. 18, no. 2, pp. 601–605, Apr. 2019.

[9] W. Lee, Y. K. Hong, J. Lee, and D. Gillespie, "Dual-polarized hexaferrite antenna for unmanned aerial vehicle (UAV) applications," *IEEE Antennas Wireless Propag. Lett.*, vol. 12, pp. 765–768, 2013.

[10] Z.-Q. Liu, Y.-S. Zhang, Z. Qian, Z. P. Han, and W. Ni, "A novel broad beamwidth conformal antenna on unmanned aerial vehicle," *IEEE Antennas Wireless Propag. Lett.*, vol. 11, pp. 196–199, 2012.

[11] Y. Zeng, R. Zhang, and T. J. Lim, "Wireless communications with unmanned aerial vehicles: Opportunities and challenges," *IEEE Commun. Mag.*, vol. 54, no. 5, pp. 36–42, May 2016.

[12] I. J. Nam, S. M. Lee, and D. H. Kim, "Miniaturized beam reconfigurable reflectarray antenna with wide 3-D beam coverage," *IEEE Trans. Antennas Propag.*, vol. 70, no. 4, pp. 2613–2622, Apr. 2022.

[13] J. Tak and J. Choi, "A flush-mounted monopolar patch antenna for UAV applications," *Microw. Opt. Technol. Lett.*, vol. 59, no. 5, pp. 1202–1207, May 2017.

[14] N. Neveu, Y.-K. Hong, J. Lee, J. Park, G. Abo, W. Lee, and D. Gillespie, "Miniature hexaferrite axial-mode helical antenna for unmanned aerial vehicle applications," *IEEE Trans. Magn.*, vol. 49, no. 7, pp. 4265–4268, Jul. 2013.

[15] Z. Liang, Z. Liang, Y. Li, J. Liu, J. Qin, and Y. Long, "Reconfigurable microstrip magnetic dipole antenna with switchable conical beams for aerial drone applications," *IEEE Access*, vol. 7, pp. 31043–31054, 2019.

[16] H. Xu, J. Cui, J. Duan, B. Zhang, and Y. Tian, "Versatile conical conformal array antenna based on implementation of independent and endfire radiation for UAV applications," *IEEE Access*, vol. 7, pp. 31207–31217, 2019.

[17] X. L. Guo, H. B. Ji, H. H. Yin, and J. Huang, "Antenna for wireless communications on unmanned aerial vehicles," *Appl. Mech. Mater.*, vols. 241–244, pp. 2487–2490, Dec. 2012.

[18] J. M. Inclán Alonso and M. S. Pérez, "Phased array for UAV communications at 5.5 GHz," *IEEE Antennas Wireless Propag. Lett.*, vol. 14, pp. 771–774, 2015.

[19] K.-S. Kim, J.-S. Yoo, J.-W. Kim, S. Kim, J.-W. Yu, and H. L. Lee, "All-around beam switched antenna with dual polarization for drone communications," *IEEE Trans. Antennas Propag.*, vol. 68, no. 6, pp. 4930–4934, Jun. 2020.

[20] Y.-S. Choi, J.-S. Park, and W.-S. Lee, "Beam-reconfigurable multi-antenna system with beam-combining technology for UAV-to-everything communications," *Electronics*, vol. 9, no. 6, p. 980, Jun. 2020.

[21] D. G. Seo and W. S. Lee, "A multiply parasitic-coupled, three-dimensional antenna array with wide elevation angle for seamless UAV communications," *Appl. Comput. Electromagn. Soc. J.*, vol. 35, no. 4, pp. 461–465, Apr. 2020.

[22] D. G. Seo, J. S. Park, G. K. Lee, and W. S. Lee, "Lightweight printed dipole antenna array with 3×2 beamforming network for wide UAV communication coverage," *J. Elect. Eng. Technol.*, vol. 15, no. 4, pp. 1769–1773, Jul. 2020.

[23] Y.-Y. Jeong and W.-S. Lee, "Wideband printed half bow-tie antenna array based on a quad-mode reconfigurable feeding network for UAV communications," *IEEE Open J. Antennas Propag.*, vol. 2, pp. 238–248, 2021.

[24] *CST Microwave Studio*. Accessed: 2019. [Online]. Available: http://www.cst.com/

[25] C. A. Balanis, *Antenna Theory: Analysis and Design*. 3rd ed. New York, NY, USA: Wiley, 2005, pp. 284–302.

[26] J. L. Salazar, A. Umeyama, S. Duthoit, and C. Fulton, "UAS-based antenna pattern measurements and radar characterization," in *Proc. IEEE Conf. Antenna Meas. Appl. (CAMA)*, Sep. 2018, pp. 1–4.

[27] A. Y. Umeyama, J. L. Salazar-Cerreno, and C. J. Fulton, "UAV-based far-field antenna pattern measurement method for polarimetric weather radars: Simulation and error analysis," *IEEE Access*, vol. 8, pp. 191124–191137, 2020.
[28] A. Y. Umeyama, J. L. Salazar-Cerreno, and C. Fulton, "UAV-based antenna measurements for polarimetric weather radars: Probe analysis," *IEEE Access*, vol. 8, pp. 191862–191874, 2020.
[29] *Broadband SPDT RF Switch*, CG 2430X3 Datasheet, Californai Eastern Laboratories, Santa Clara, CA, USA, Aug. 2017.
[30] *SKY13408-465LF: 1.0 to 6.0 GHz SP3T Switch, 50 Ω Terminated*, SKY13408-465LF Datasheet, Skyworks, Irvine, CA, USA, Sep. 2015.
[31] *90 deg Hybrdi Couplers*, CMX55Q03 Datasheet, RN2 Technologies, Seoul, South Korea, Apr. 2017.

YE-YEONG JEONG received the B.S. and M.S. degrees in electronic engineering from Gyeongsang National University (GNU), Jinju, South Korea, in 2019 and 2021, respectively.

Her current research interests include wide beam coverage antenna, beamforming antenna array and its feeding network for UAV communications, RF/Microwave circuit and systems, and RFID/IoT sensors.

SEONG-HYEOP AHN (Student Member, IEEE) received the B.S. and M.S. degrees in electronic engineering from Gyeongsang National University (GNU), Jinju, South Korea, in 2018 and 2020, respectively.

His research interests include high-power microwave systems, near-field wireless power transfer and communications systems, RFID/IoT sensors, and RF/microwave circuit and antenna designs.

JINHWAN KOH (Member, IEEE) received the B.S. degree in electronics from Inha University, Incheon, South Korea, and the M.S. and Ph.D. degrees in electrical engineering from Syracuse University, Syracuse, NY, USA.

He is currently a Professor with the Department of Electronic Engineering, Engineering Research Institute, Gyeongsang National University, Jinju, South Korea. His current research interests include radar signal processing and electromagnetic measurement.

WANG-SANG LEE (Senior Member, IEEE) received the B.S. degree from Soongsil University, Seoul, South Korea, in 2004, and the M.S. and Ph.D. degrees in electrical engineering from the Korea Advanced Institute of Science and Technology (KAIST), Daejeon, South Korea, in 2006 and 2013, respectively.

From 2006 to 2010, he was with the Korea Testing Laboratory (KTL), Digital Industry Division, Electromagnetic Compatibility Technology Center, Ansan-si, South Korea, where he was involved in the international standardization for radio frequency identification (RFID) and photovoltaic systems as well as electromagnetic interference (EMI)/EMC analysis, modeling, and measurements for information technology devices. In 2013, he joined the Korea Railroad Research Institute (KRRI), Uiwang-si, South Korea, as a Senior Researcher, where he was involved in the position detection for high-speed railroad systems and microwave heating for low-vibration rapid tunnel excavation system. Since 2014, he has been an Associate Professor with the Department of Electronic Engineering, Gyeongsang National University (GNU), Jinju, South Korea. From 2018 to 2019, he was a Visiting Scholar with the ATHENA Group, Georgia Institute of Technology, Atlanta, GA, USA. His current research interests include near- and far-field wireless power and data communications systems, RF/microwave antenna, circuit, and system design, RFID/Internet of Things (IoT) sensors, and EMI/EMC.

Dr. Lee is a member of IEC/ISO JTC1/SC31, KIEES, IEIE, and KSR. He was a recipient of the Best Paper Award from IEEE RFID, in 2013, the Kim Choong-Ki Award–Electrical Engineering Top Research Achievement Award from the Department of Electrical Engineering, KAIST, in 2013, the Best Ph.D. Dissertation Award from the Department of Electrical Engineering, KAIST, in 2014, the Young Researcher Award from KIEES, in 2017, and the Best Paper Awards at IEIE, in 2018, and KICS, in 2019.